Effect of Varying Composition on Temperature Reconstructions Obtained from Refractive Index Measurements in Flames

XIAO QIN, XUDONG XIAO, ISHWAR K. PURI,* and SURESH K. AGGARWAL
Department of Mechanical Engineering (M/C 251), University of Illinois at Chicago, 842 W. Taylor St., Chicago, IL 60607-7022, USA

Optical methods (such as holographic interferometry, speckle photography, speckle shearing interferometry, moiré deflectometry, rainbow Schlieren deflectometry and Talbot interferometry, and so forth) have the potential for accurately measuring the entire temperature field associated with multidimensional flames, which may be difficult to do using other techniques. These interferometric or deflectometric techniques first determine the refractive index in flames, and thereafter infer the temperature distribution. The relationship between the refractive index and temperature is obtained by using a state equation and the Gladstone–Dale relation. However, a potential source of error arises since the local composition of the flame being studied is usually unknown. In a previous investigation, we examined the occurrence of this error by assuming the local flame composition to be the same as that of air at the local temperature. This was examined through one–dimensional simulations of counterflow flames. We found that while calculating the temperature from the measured refractive index this assumption could lead to significant errors for some flames and to minimal errors in other flames. This investigation quantifies those errors in the context of two–dimensional flames in both planar and axisymmetric geometries. It is found that the refractive index values of a mixture are nearly identical with those of the refractive index of air for partially premixed flames (PPFs). The maximum error lies in the range of 6.3 to 10.7% for one–dimensional (1–D) counterflow PPFs, and between 6.1 to 8.0% for two–dimensional (2–D) planar and axisymmetric PPFs (for equivalence ratios in the range of $1.5 \leq \phi_r \leq 2.0$). For nonpremixed flames, however, the maximum error can have values up to 33.8% and 34.5% for the 1–D and 2–D configurations, respectively. Therefore, the accurate inference of the temperature of nonpremixed flames from the measured refractive index distribution requires that an alternative approach be developed. We have developed an interpolation method that reduces the maximum error from 34.5% to 9.8% for these flames, and is associated with even smaller errors in most other regions of these flames.

INTRODUCTION

Optical methods, such as holographic interferometry, speckle photography, speckle shearing interferometry, moiré deflectometry, rainbow Schlieren deflectometry and Talbot interferometry, and so forth have the potential for measuring accurately the complete temperature field associated with multidimensional flames that may be difficult to do using other techniques. Shaker and Nirala [1] discussed the advantages and disadvantages of the above techniques for measuring temperature profiles in a recent review. Some techniques are also described in details in comprehensive discussion. For instance, Vest [2] has elaborated the theory, practice and application of holographic interferometry, and Cloud [3] has provided an up-to-date exposition of optical methods (speckle photography, electronic speckle pattern interferometry, phase-shifting interferometry, and so forth) in engineering analyses. These nonintrusive diagnostic techniques first determine the refractive index in flames, and thereafter infer the temperature distribution. The relationship between refractive index and temperature is obtained by using a state equation and the Gladstone–Dale (G–D) relation. However, a potential source of error arises since the local composition of the flame being studied is usually unknown. This error is different from other types of errors encountered when measuring the refractive index in flames. The sources of other experimental errors can be generally divided into two categories: those associated with the measurement system geometry, and those associated with measuring the optical phase. Both of these experimental errors can be severe when making refractive index measurements and can produce large discrepancies. The first kind of

*Corresponding author. E-mail: ikpuri@uic.edu

COMBUSTION AND FLAME 128:121–132 (2002)

Published by Elsevier Science Inc.
0010-2180/02/$–see front matter
PII 0010-2180(01)00338-8

error can be minimized or even eliminated through a careful setup of the optical system. Use of higher-accuracy equipment can minimize the latter error.

The effect of varying composition has usually been neglected in most applications of interferometric or deflectometric techniques employed to measure the temperatures in reacting flows [4–7]. Keren et al. [8] demonstrated the mapping of temperature in a premixed hydrogen-oxygen flame by moiré deflectometry, and only used the refractivities of major species (water, hydrogen, and oxygen) to reconstruct the flame temperature. South and Hayward [9] measured temperature distribution in an axisymmetric nonpremixed methane-air flame using holography interferometry and argued that at atmospheric pressure most of the refractive index variation is because of a temperature change. They stated that the effect of diffusion–induced changes in composition is pronounced only in the early part of the temperature rise when the local temperature is a small fraction of the peak flame temperature. Tieng and coworkers studied the effect of composition on the measurement accuracy for two laminar propane–air flames, that is, a fuel-lean premixed flame [10] and a nonpremixed flame [11]. They concluded that the composition effect is less significant in case of the lean premixed flame, but is very important in the lower spatial section of the nonpremixed flame.

Motivation

In a previous investigation [12], we characterized the effect of equivalence ratio ϕ on refractivity using the simulation results of one–dimensional (1–D) partially premixed flames (PPFs) established in a counterflow configuration at a moderate strain rate a = 50 s^{-1}. We found that the errors were relatively small for relatively rich partially premixed flames (up to $\phi = 2.0$), but were significant in case of the nonpremixed flame. However, realistic flames occur in multidimensional configurations, and heat and mass transport effects (e.g., through molecular diffusion) are more severe in this case. Therefore, it is necessary to further investigate the effect of varying composition on temperature reconstructions obtained from refractive index measurements in flames in the context of multidimensional geometries.

Objective

We have previously reported successful simulations of partially premixed flames stabilized both on a slot burner [13, 14] and on an axisymmetric co-annular burner [15, 16]. Validation of the computational code in terms of reaction zone topology, flow velocity fields, temperature and the streamwise species concentration profiles have been presented in those papers. Within the range of computational and experimental errors, we have found good qualitative and quantitative agreement between the measurements and simulations. Because of the difficulties associated with accurately measuring the local composition in flames, it is reasonable to use the simulation results of two–dimensional (2–D) planar and axisymmetric methane–air partially premixed flames to evaluate the refractive index spatial distribution.

This investigation employs detailed numerical simulations to quantify errors in the reconstruction of temperature from a specified or measured refractive index distribution in 2-D flames that are established in planar and axisymmetric configurations. We have previously found that the maximum errors lie in the range of 6.3 to 10.7% for 1–D counterflow PPFs (depending upon their stoichiometry). We show that the corresponding errors lie between 6.1 to 8.0% for 2–D planar and axisymmetric PPFs (for equivalence ratios in the range $1.5 \leq \phi_r \leq 2.0$). For nonpremixed flames, however, the maximum error can have values up to 33.8% and 34.5% for the 1–D (as previously determined) and 2–D (as found herein) configurations, respectively. Therefore, the inference of temperature from the measured refractive index for nonpremixed flames requires that an alternative approach be developed. We will present an interpolation method that reduces the maximum temperature error from 34.5% to 9.8%, and is associated with even smaller errors in most regions of the flames.

Refractive Index in Flames

The relationship between the refractive index and temperature can be determined by using

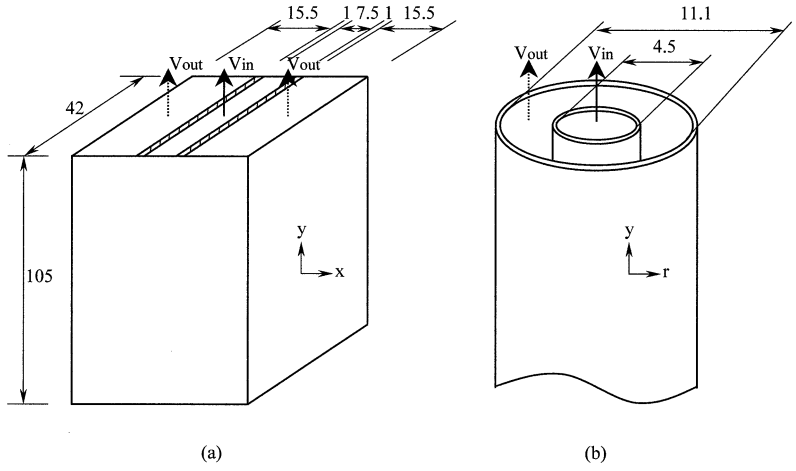

Fig. 1. Schematic diagram of (a) the slot burner, and (b) the axisymmetric co-annular burner. Dimensions are in units of mm

the ideal gas law and the G–D relation [2]. The ideal gas law for a mixture has the form

$$\rho(x,y,z) = (P/R)(W_{mix}(x,y,z)/T(x,y,z)), \qquad (1)$$

where $\rho(x,y,z)$ denotes the mass density at a position (x,y,z), T(x,y,z) the absolute temperature, P the pressure, R the universal gas constant, and $W_{mix}(x,y,z)$ the mixture molecular weight. The molecular weight can be expressed as

$$w_{mix}(x,y,z) = (\Sigma Y_i(x,y,z)W_i^{-1})^{-1}, \qquad (2)$$

where Y_i and W_i, respectively, represent the mass fraction and molecular weight of the i–th species, and Σ denotes summation over all the species that are present. The dependence of the refractive index on density is obtained from the G–D relation, that is,

$$n(x,y,z)-1 = \rho(x,y,z)K_{mix} = \rho(x,y,z)(\Sigma Y_i(x,y,z)k_i), \qquad (3)$$

where n(x,y,z) denotes the refractive index, k_i the G–D constant for the i–th species, and $K_{mix} = \Sigma Y_i(x,y,z)k_i$. The temperature can be related to the refractive index by combining Eqs. 1–3, that is,

$$T(x,y,z) = [n(x,y,z)-1]^{-1}\beta(x,y,z), \qquad (4)$$

where $\beta(x,y,z) = (P/R)[\Sigma Y_i(x,y,z)k_i][\Sigma Y_i(x,y,z)W_i^{-1}]^{-1}$ is the refractivity.

The temperature T(x,y,z) can be obtained relative to some reference temperature T_0, at which the refractive index n0 has a known value, that is,

$$T(x,y,z) = T_0(n_0 - 1)/(n(x,y,z) - 1), \qquad (5)$$

Unfortunately, Eq. 5 is not suitable unless the local composition in the flame is known. Therefore, $\beta(x,y,z)$ is often assumed constant throughout the flame, for example, by assuming the local composition to correspond to that of air [2]. The justification for doing so is that in many flames, particularly those established through partially premixed or fully premixed combustion, air is used both a diluent and a reactant. Since air consists overwhelmingly of nitrogen, the properties of $\beta(x,y,z)$ approach its value for nitrogen. With such an assumption,

$$T(x,y,z) = T_0(n_0 - 1)/(n(x,y,z) - 1), \qquad (6)$$

The present investigation uses Eqs. 5 and 6 and the detailed numerical simulations to quantify errors in temperature reconstructions from the given refractive index distributions in 2-D planar and axisymmetric flames.

PHYSICAL–NUMERICAL MODEL

The physical model considers a laminar partially premixed flame that contains two reaction zones. The flame is stabilized either on a Wolfhard–Parker slot burner or on an axisymmetric co-annular burner. The schematic diagrams of

TABLE 1

Relevant gas parameters required to calculate refractive index n(x,y)

Species	Molecular Weight (kg kmol^{-1})	k $\times$ 10^{-4} (m^3 kg^{-1})
CH_4	16.04	6.15
O_2	32.00	1.89
H_2O	18.02	3.12
CO_2	44.01	2.26
CO	28.00	2.67
H_2	2.02	1.54
O	16.00	1.73
H	1.01	25.63
C_2H_2	26.02	5.05
C_2H_4	28.04	5.69
C_2H_6	30.06	5.63
N_2	28.01	2.38
Air	28.97	2.26

the two burners are presented in Fig. 1. The slot burner has an inner slot and two symmetric outer slots. A fuel–rich methane–air mixture is introduced from the inner slot and air is introduced from the two symmetric outer slots. The axisymmetric co-annular burner consists of an inner tube and a concentric outer tube.

The computational model is based on the algorithm developed by Katta et al. [17]. An implicit algorithm is employed to solve the unsteady gas–phase equations. The simulation method is described in detail elsewhere [18, 19]. The numerical model solves the time–dependent governing equations for 2–D planar or axisymmetric reacting flows. These equations representing the mass, momentum, species, and energy conservation equations can be written in the generalized form as

$$\frac{\partial(\rho\phi)}{\partial t} + \frac{\partial(\rho u\phi)}{\partial x} + \frac{\partial(\rho v\phi)}{\partial y} = \frac{\partial}{\partial x}\left(\Gamma^{\phi}\frac{\partial\phi}{\partial x}\right) + \frac{\partial}{\partial y}\left(\Gamma^{\phi}\frac{\partial\phi}{\partial y}\right) + S^{\phi}, \quad (7)$$

where ρ denotes the density, and u and v the transverse or radial (x or r) and the axial (y) velocity components, respectively. The transport coefficient Γ^{Φ} and the source terms S^{Φ} appearing in the governing equations are provided in Table 1 of Ref. 14. The set of equations is completed by introducing the mass conservation equation and the state equation $p = \rho RT\Sigma_i Y_i/W_i$. The thermodynamic and transport properties appearing in the above equations are considered to be temperature–and species–dependent. The methodology to calculate these properties are described elsewhere [15]. The methane–air chemistry is modeled using a relatively detailed reaction mechanism that considers 24 species and 81 elementary reactions [20].

The computational domain is bounded by the symmetry plane (or axis of symmetry) and an outflow boundary in the transverse (or radial) direction and by the inflow and another outflow boundary in the axial direction. Symmetric conditions are applied at the left boundary, while those at the right boundary correspond to a free surface. The outflow boundaries in both directions are located sufficiently far from the respective inflow and symmetric boundaries so that the propagation of boundary–induced disturbances is minimized. The boundary conditions are chosen to match the experiments. The governing equations are integrated by using a "finite control volume" approach with a staggered, nonuniform 121 $\times$ 61 grid system. Validation of the computational code in terms of the reaction zone topography, the flow velocities, and the temperature distributions has already been presented earlier [13–16, 21]. The grid independence of the numerical results is discussed in Ref. [22].

RESULTS AND DISCUSSION

Global Flame Structure

We have shown that the flame structure of complex partially premixed flames in various configurations follows state relationships with respect to a modified conserved scalar (also called the modified mixture fraction) $\xi = (Z–Z_l)/(Z_r–Z_l)$ [19], although the approach assumes equal diffusivity of all species [23, 24]. Here Z denotes the relative local mass fraction originating in the fuel, and the subscripts r and l are conditions relevant at the boundaries of the rich and lean regions, respectively. The use of ξ transforms the system–specific spatial coordinate system into a generic, universally applicable coordinate. In a generic partially premixed

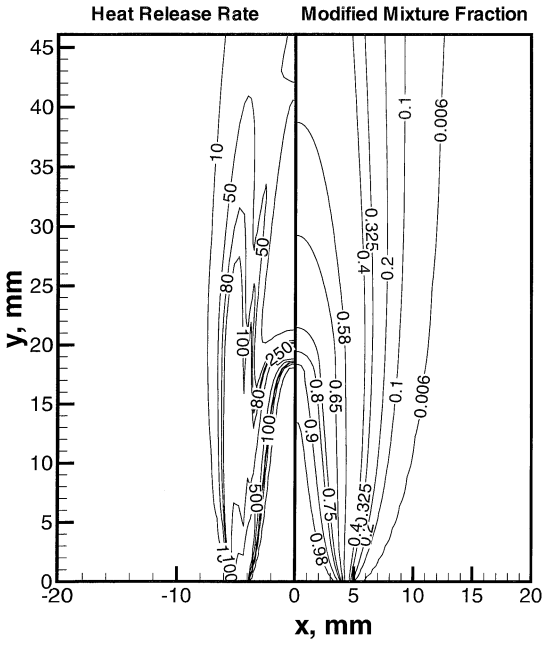

Fig. 2. Methane–air partially premixed flame structure in terms of heat release rate (units: kJ kg^{-1} s^{-1}) and modified mixture fraction contours. Equivalence ratios are $\phi_r = 2.0$, and $\phi_l = 0$, and the mean flow velocity is 0.3 m s^{-1} in both the inner and outer streams.

flame, the lean side equivalence ratio (at $\xi = 0$) is ϕ_l, and the rich side ratio (at $\xi = 1$) is ϕ_r.

Figure 2 presents the contours of heat release rate (left) and modified mixture fraction (right) for a typical methane–air partially premixed flame stabilized on the Wolfhard–Parker slot burner at equivalence ratios $\phi_r = 2.0$, and $\phi_l = 0$. The mean velocity at the slot exit for both inner and outer streams is 0.3 m s^{-1}. Both sets of contours represent the flame shape clearly, suggesting a strong correlation between the heat release and modified mixture fraction. From the heat release rate contours, it is evident that the flame contains two reaction zones, one a rich premixed zone, and the other a nonpremixed zone. We have previously reported good agreement between the C_2^* chemiluminescence emission intensity, which is a good indicator of the reaction zone topology, and the computed volumetric heat release rate for partially premixed flames [13, 21]. From the modified mixture fraction contour, the rich premixed reaction can be characterized as lying in the range $0.75 < \xi < 0.9$, while the nonpremixed reaction zone is located in the range $0.25 < \xi < 0.5$.

Figure 3 presents the state relationships in terms of temperature and mass fraction of CH_4, CO, and H_2O that are plotted with respect to the modified mixture fraction for the flame corresponding to Fig. 2. The maximum temperature of 2141 K occurs at $\xi = 0.55$ (cf. Fig. 3a), which lies between the rich premixed and nonpremixed reaction zones. The temperature plots corresponding to the modified mixture fraction values smaller than 0.55 generally fall on a single curve, while those for $\xi > 0.55$ show some scatter, which is also observed in the state relationships for CH_4, CO, and H_2O mass fraction. The scatter occurs because of two–dimensional transport and chemistry effects [19] and because of the upstream interaction that occurs between the nonpremixed and the rich premixed reaction zones near the "double point" at the flame base.

From Fig. 3b we note that when ξ has values less than 0.65, methane is almost completely consumed in the nonpremixed reaction zone. This clearly suggests that methane is not the primary fuel for the nonpremixed reaction zone, and that other intermediate products serve as fuel (namely, carbon monoxide and molecular hydrogen) and react with the oxidant being transported from the air stream. It is seen from Figs. 3c and 3d that the maximum mass fraction of CO or H_2O occurs in the rich premixed zone. Both CO and H_2 are mainly produced in the rich premixed reaction zone, and then transported to the nonpremixed reaction zone and consumed there.

Refractive Index Distribution

The local refractive index can be determined as a function of temperature and composition at any location. The relevant gas parameters that are required to calculate n(x,y,z) are listed in Table 1. Only the major species are considered in the refractive index calculation so that there is an "omitted mass fraction" of minor species for which Gladstone–Dale constant values are not available in the literature. The mass fraction of omitted minor species is quite small. For example, the maximum value of the omitted mass fraction is 0.44% for the flame corresponding to Fig. 2. Therefore, it is reasonable to assume that neglecting such a small fraction of

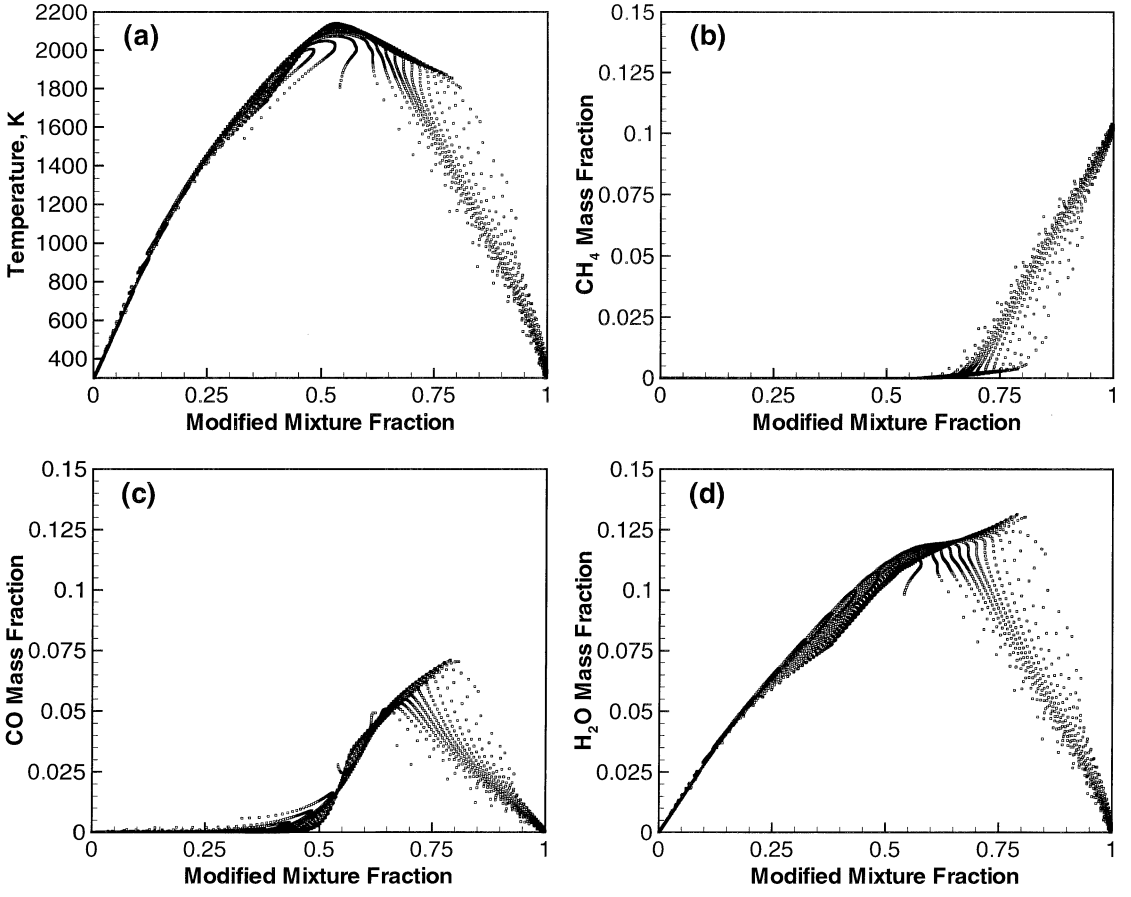

Fig. 3. Figure 3 State relationships in terms of temperature (a), and CH_4 (b), CO (c), and H_2O (d) mass fraction, with respect to modified mixture fraction for the flame corresponding to Fig. 2.

the species that are present locally does not significantly influence the calculated value of n(x,y,z).

Figure 4 presents the refractive index distribution as a function of the modified mixture fraction for three planar (slot burner) flames (cf. Figs. 4a–c) corresponding to different levels of partial premixing (ϕ_r = 1.5, 1.7, and 2.0, respectively), and for a nonpremixed flame (cf. Fig. 4d). The mean velocity at the slot exit for both inner and outer streams is 0.30 m s^{-1} for PPFs, and 0.10 m s^{-1} for the nonpremixed flame. Figure 5 shows the refractive index distribution as a function of the modified mixture fraction for the corresponding axisymmetric (concentric burner) PPFs (cf. Figs. 4a–c), and for a nonpremixed flame (cf. Fig. 4d). The inner and outer mean velocities for axisymmetric PPFs are 0.6 m s^{-1} and 0.5 m s^{-1}, respectively, and those for the nonpremixed flame are 0.10 m s^{-1}. The refractive index distribution for the corresponding counterflow (1–D) flames is also shown in Figs. 4 and 5.

Each case contains two values of the refractive index, one $n_{mix}(Y_i,T,x,y)$ that is based on the actual composition and the local temperature, and the other $n_{air}(T,x,y)$ that is based on the assumption that the mixture composition is the same as that of air, but at the local temperature. The smallest refractive index values occur in the high temperature region of the flame. In Figs. 4a–c and 5a–c, the values of $n_{mix}(x,y)$ are virtually identical with those of $n_{air}(x,y)$ for the three partially premixed flames in both counterflow (1–D) and co-flow (2–D planar and axisymmetric) configurations. The refractive indices for 1–D and 2–D flames are in good agreement for modified mixture fraction values lower than

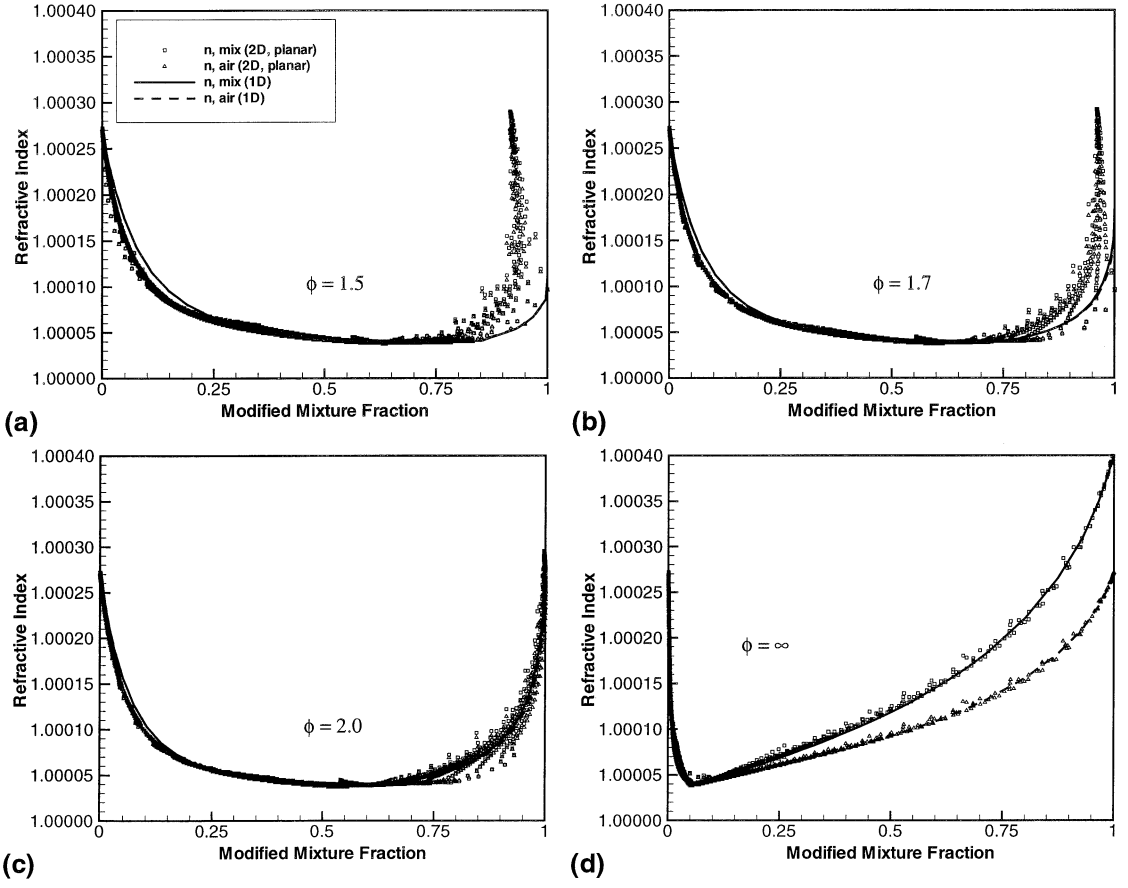

Fig. 4. Figure 4 Refractive index distribution as a function of modified mixture fraction for three planar (slot burner) partially premixed flames (a–c) corresponding to different levels of partial premixing (ϕ_r = 1.5, 1.7, and 2.0), and for a nonpremixed flame (d). The mean flow velocity in both inner and outer streams is 0.3 m s^{-1} for the three partially premixed flames, and 0.1 m s^{-1} for the nonpremixed flame. The refractive index distributions for the corresponding counterflow (1–D) flames at a strain rate of 50 s^{-1} are also presented.

0.75. However, for $\xi > 0.75$, the refractive index distributions for the 2–D flames show scatter. This is related to the scatter in temperature and composition in the fuel rich premixed reaction zone, which has been discussed above in the context of Fig. 3. For the flames corresponding to Fig. 2, the maximum relative error is 0.0024% and it occurs in the rich premixed zone. In Figs. 4d and 5d, $n_{mix}(x,y)$ and $n_{air}(x,y)$ deviate significantly for modified mixture fraction values above 0.25. This discrepancy arises because of the composition difference in the nonpremixed reaction zone where methane replaces nitrogen and oxygen.

Comparing Figs. 4 and 5, we can see that despite the configurational difference between the planar and axisymmetric 2–D flames, the values of refractive indices for all the cases considered are in good agreement with respect to the modified mixture fraction. We see from Figs. 4a and 5a that relatively large discrepancies between the 1–D and 2–D configurations occur in the inner rich premixed zone. Choi and Puri [25] have observed that the range of flame stretch effects for axisymmetric flames is broader than that for planar flames and, thus, the flame temperature and refractive index exhibit even more severe scatter. The results for 1–D flames are obtained at a moderate strain rate a = 50 s^{-1}. For the 2–D flames, because of to flame stretch effects in the inner premixed zone, their behavior corresponds to a set of different 1–D flames at a strain rate other than

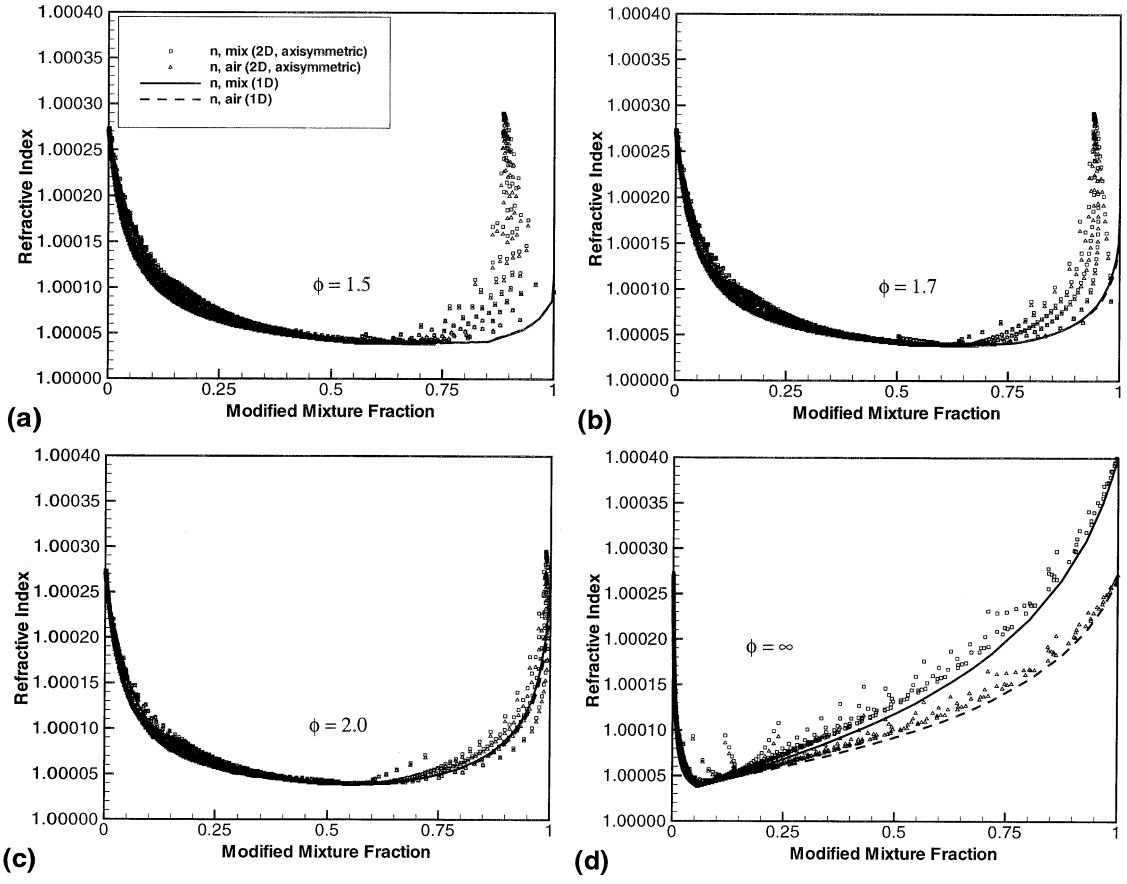

Fig. 5. Refractive index distribution as a function of modified mixture fraction for three axisymmetric partially premixed flames (a–c) corresponding to various levels of partial premixing (ϕ_r = 1.5, 1.7, and 2.0), and for a nonpremixed flame (d). The inner and outer stream mean velocities are of 0.6 m s^{-1} and 0.5 m s^{-1}, respectively, for the three partially premixed flames, and 0.1 m s^{-1} for the nonpremixed flame.

50 s^{-1}. The discrepancy between 1–D and 2–D configuration becomes smaller with an increase in the equivalence ratio.

Reconstructed Temperature

Using Eq. 6, the temperature field can be reconstructed from the refractive index distribution. The assumption of constant $\beta(x,y)$ in Eq. 4 introduces an error in calculating the local temperature. Here, the average and maximum errors, denoted as E_{av} and E_{max} respectively, are defined as:

$$E_{av} = \sqrt{\frac{\Sigma\, e_i^2}{J}} \text{ and } E_{max} = \text{maximum value of } |e_i|, \quad (8)$$

where $e_i = T_{1i} - T_i$ denotes the local error, T_{1i} the local value of temperature calculated from Eq. 6, T_i the temperature value from simulation results, and J the number of points in the domain. The average and maximum errors are in the range of 2.4 to 4.9% and 6.3 to 10.7%, respectively, for 1–D PPFs, and 1.7 to 2.3% and 6.1 to 8.0%, respectively, for 2–D PPFs. The average and maximum errors for the nonpremixed 1–D flame are 12.3% and 33.8%, respectively, while the corresponding errors for the 2–D planar nonpremixed flame are, respectively, 7.2% and 33.3%. Therefore, while the assumption of constant $\beta(x,y)$ introduces small errors in interferometric or deflectometric temperature measurements in case of PPFs, this assumption can lead to significantly large discrepancies of nonpremixed flames.

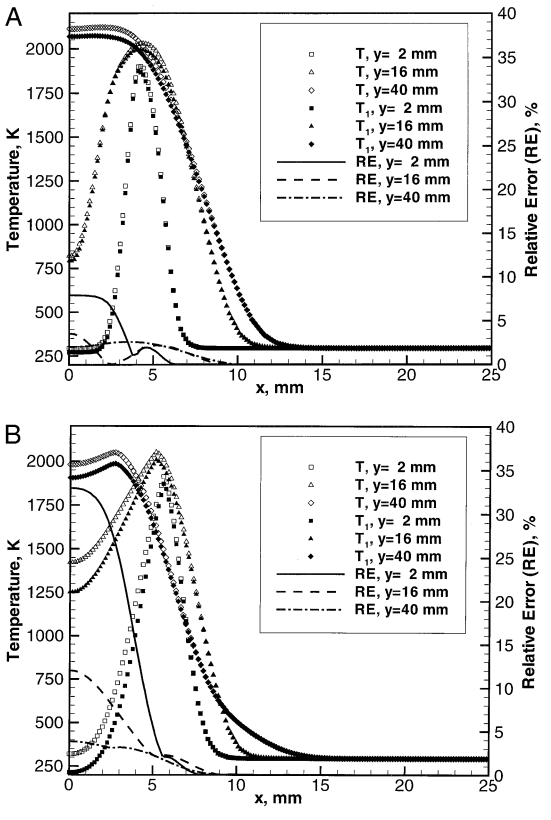

Fig. 6. Temperature profiles in the transverse direction plotted at three different axial cuts for the planar partially premixed flame (a) with $\phi_r = 2.0$ corresponding to Fig. 2(a), and the nonpremixed flame (b) corresponding to Fig. 4d. Here, T denotes the temperature calculated using Eq. 4, and T_1 the temperature from simulations. Relative errors (RE) at the corresponding locations are also shown.

Figures 6a and 6b show the temperature distribution for the planar flame for which $\phi_r = 2.0$ (corresponding to Fig. 2) and for a nonpremixed flame ($\phi_r = \infty$), respectively. The temperature distribution is shown at three different axial locations (y = 2 mm, 16 mm, and 40 mm). The relative errors at the corresponding locations are also shown. Large deviations are observed along the centerline of the flame and the flame front where the hydrocarbon concentrations change rapidly. At higher axial locations in the flame (y = 40 mm), the two temperatures T_1 and T are in good agreement and the relative errors are small. The temperatures reconstructed by Eq. (6) have lower values than those obtained from the simulations because of the replacement of methane by air (the G–D constant for which has a lower value).

We observe from Fig. 6a that the occurrence of a nonpremixed reaction zone outside the inner rich premixed zone does not introduce large errors into the temperature reconstruction, although the errors do increase somewhat in this region. The nonpremixed reaction zone in partially premixed flames is established because of the consumption of intermediate products (e.g., carbon monoxide and molecular hydrogen) that are transported from the inner rich premixed reaction zone, and which produce water and carbon dioxide. The G–D constant values for these intermediate species are nearly the same as those for air. Therefore, the species do not influence the value of refractive index of the mixture as significantly as does methane in the inner reaction zone. Figure 6b clearly illustrates the effect of methane concentration on the temperature reconstruction in the inner premixed reaction zone. The maximum relative error at the centerline 2-mm above the burner exit is 33.3%. The error decreases rapidly at higher axial locations. For instance, the relative error along the centerline reduces to 11.8% and 3.8% at displacements y = 16 mm and 40 mm, respectively. This indicates that composition effects are significant for nonpremixed flames in the context of temperature reconstruction only in the lower regions of the fuel jet.

Temperature Correction

To correct the errors introduced by composition effects for nonpremixed flames, it is necessary to reconsider Eq. 5. Without knowing the concentration distribution of the species, it is difficult to apply Eq. 5 directly. However, since methane dominates the composition of the mixture in the lower portion of the fuel jet of a nonpremixed flame, we can use the methane concentration to approximate the value of $\beta(x,y)$ for the mixture.

Figure 7 presents the methane mass fraction profiles at different transverse (cf. Fig. 7a) and axial (cf. Fig. 7b) locations for the planar nonpremixed flame corresponding to Fig. 4d. In Fig. 7a, we can see that along the axial coordinate, the methane mass fraction decays exponentially. From Fig. 7b we see that the methane mass fraction decreases approximately linearly along the transverse coordinate and reaches a value close to zero at about x = 5.5 mm. The data

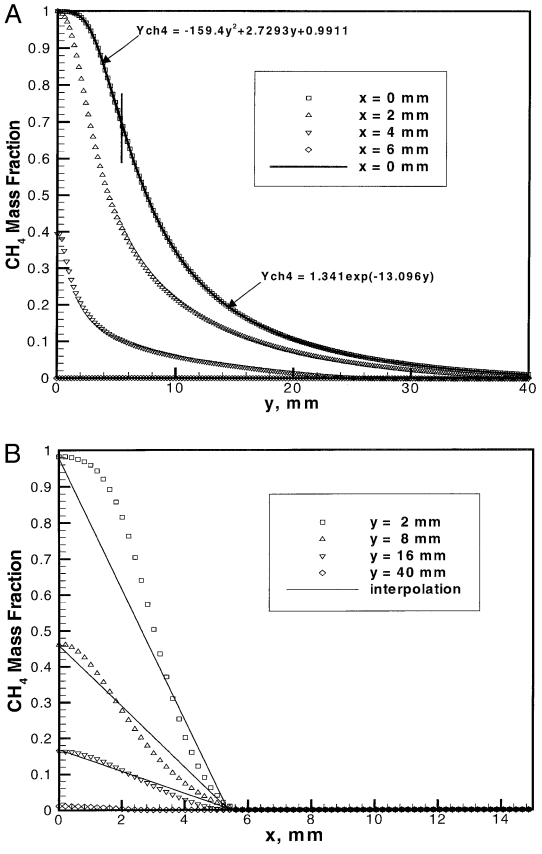

Fig. 7. Methane mass fraction profiles at different transverse (a) and axial (b) locations for the planar nonpremixed flame corresponding to Fig. 4(d).

shows that along the symmetry line (x = 0 mm) in Fig. 7a, the following regression function applies, i.e.,

$$\begin{cases} Y_{CH4,0} = -159.4y^2 + 2.7293y + 0.9911, & x \le 0.05\ \text{m} \\ Y_{CH4,0} = 0 \qquad\qquad\qquad\qquad\quad , & y > 0.05\ \text{m} \end{cases} \tag{9}$$

where $Y_{CH4,0}$ denotes the methane mass fraction along the axis. Subsequently, using the value of $Y_{CH4,0}$, we can linearly interpolate along the transverse coordinate and obtain the relation

$$\begin{cases} Y_{CH4,i} = Y_{CH4,0}(0.055 - x)/0.55, & x \le 0.055\ \text{m} \\ Y_{CH4,i} = 0 \qquad\qquad\qquad\quad , & x > 0.055\ \text{m} \end{cases} \tag{10}$$

Next, the values of $\beta(x,y)$ for the mixture are approximated by the equation

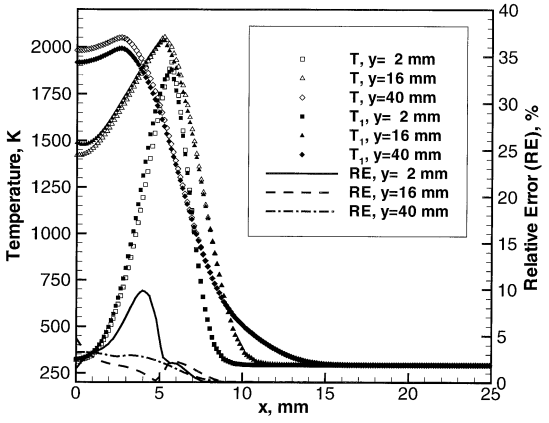

Fig. 8. Temperature distribution for the nonpremixed flame corresponding to Fig. 4(d), where the reconstructed temperature T_1 is calculated by interpolation method.

$$K_{mix} = Y_{CH4,i}\, k_{CH4} + (1 - Y_{CH4})k_{air}, \tag{11}$$

$$W_{mix} = [Y_{CH4,i}/W_{CH4} + (1 - Y_{CH4})/W_{air}]^{-1}, \tag{12}$$

$$\beta(x, y) = PK_{mix}W_{mix}/R, \tag{13}$$

Substituting the above relation for $\beta(x,y)$ into Eq. 5 and using the value of $\beta_0 = 0.079945$ for air at atmospheric pressure and room temperature (295 K), the resulting calculated temperature profiles are presented in Fig. 8. The errors are largely reduced, specially close to the centerline. The maximum relative error is reduced to 9.8% and occurs in the vicinity of the base of the flame where the composition change regarding methane is difficult to express through a simple linear interpolation.

To apply the above method, the methane fuel mass fraction profiles along the axis has to be first determined. It is not possible to employ interferometric or deflectometric techniques to determine the composition distribution in flames. Consequently, no simple method can be used to reconstruct the temperature profiles in the lower section of a nonpremixed flame unless the species concentration at every point is otherwise measured. Xiao and Puri [26] have established a systematic approach based on holographic interferometry measurements to characterize the flame structure. They concluded that it is possible to use holographic interferometry to infer the mixture fraction distribution and thereafter the flame structures

TABLE 2

Average and maximum errors for the four cases discussed in the context of Figs. 4 and 5

	1-D Flame		2-D Flame (planar)		2-D Flame (axisymmetric)	
ϕ	E_{av}	E_{max}	E_{av}	E_{max}	E_{av}	E_{max}
1.5	2.4%	6.3%	1.7%	6.1%	1.9%	6.3%
1.7	3.4%	7.9%	1.8%	7.0%	2.0%	7.0%
2.0	4.9%	10.7%	2.1%	7.9%	2.3%	8.0%
∞	12.3%	33.8%	7.2%	33.3%	7.6%	34.5%

(i.e., the scalar distributions) in PPFs and nonpremixed flames by applying state relationships. The above interpolation method is similar, in that it reduces errors in the lower portion of nonpremixed flames by inferring the scalar (fuel concentration) distribution.

CONCLUSIONS

We have used simulations of 2–D partially premixed flames in both planar and axisymmetric configurations to determine the refractive index distribution in PPFs. The state relationships are plotted as a function of the modified mixture fraction. Because of the transport and chemical effects in 2–D flames, the refractive index distribution exhibits scatter in the fuel–rich premixed regions. Except for some minor differences, the refractive indices for 1–D counterflow flames and 2–D co-flow (planar and axisymmetric) flames have the same state relationships with respect to modified mixture fraction. Values of $n_{mix}(x,y)$ are nearly identical with those of $n_{air}(x,y)$ for the PPFs considered. The errors introduced by assuming constant $\beta(x,y)$ in calculating temperature are relatively small for partially premixed flames. As the fuel equivalence ratio increases, the error also increases. For the cases considered, the maximum error lies in the range of 6.3 to 10.7% for 1–D PPFs, and of 6.1 to 8.0% for 2–D PPFs for $1.5 \leq \phi_r \leq 2.0$. Within the bounds of computational and experimental errors, there is very good agreement between the measured and predicted temperature fields. Therefore, the simplified relationship (cf. Eq. 6) is appropriate for measuring temperatures in relatively fuel–rich partially premixed flames.

There are, however, significant discrepancies between $n_{mix}(x,y)$ and $n_{air}(x,y)$ for nonpremixed flames, which are because of the effect of composition difference in the lower flame section where methane fuel replaces nitrogen and oxygen. The maximum errors can be up to 34.5% at the axis 2-mm above the burner exit for 2–D axisymmetric flames. We have developed an interpolation method that reduces the maximum error from 34.5% to 9.8% for these flames, and is associated with even smaller errors in most regions of the flames.

This research was supported partly by the National Science Foundation Combustion and Plasma Systems Program through Grant No. CTS–9707000 for which Dr. Farley Fisher is the Program Director, and partly by the NASA Microgravity Research Division through Grant No. NCC3-688 for which Dr. Uday Hegde serves as the technical monitor.

REFERENCES

1. Shakher, C., and Nirala, A. K., *Optics and Lasers in Eng*. 31: 455–491 (1999).
2. Vest, C. M., *Holographic Interferometry* John Wiley, New York, 1979
3. Cloud, G. L., *Optical Methods of Engineering Analysis*. Cambridge University Press, 1998.
4. Montgomery, G. P., and Reuss, D. L., *Appl. Optics* 21:1373–1380 (1982).
5. Reuss, D. L., *Combust. Flame* 49:207–219 (1983).
6. Dandliker R., and Thalmann, R., *Optical Eng.* 24:824–829 (1985).
7. Farrell, P. V., and Hofeldt, D. L., *Appl. Optics* 23:1055–1059 (1984).
8. Keren, E., Bar-Ziv, E., Glatt, I., and Kafri, O., *Appl Optics* 20:4263–4266 (1981).
9. South, R., and Hayward, B. M., *Combust. Sci. Technol.* 12:183–195 (1976).

10. Tieng, S. M., Chen, C. C., and Chang K. C., *Optical Eng.* 31:353–362 (1992).
11. Tieng, S. M., Lin, C. C., Wang, Y. C., and Fujiwara, T., *Meas. Sci. Technol.* 7:477–488 (1996).
12. Xiao, X., Choi, C. W., and Puri, I. K., *Combust. Flame* 120:318–332 (2000).
13. Azzoni, R., Ratti, S., Aggarwal, S. K., and Puri, I. K., *Combust. Flame* 119:23–40 (1999).
14. Shu, Z., Krass, B. J., Choi, C. W., Aggarwal, S. K., Katta, V. R., and Puri, I. K., *Proc. Combust. Inst.* 27:625–632 (1998).
15. Shu, Z., Aggarwal, S. K., Katta, V. R., and Puri, I. K., *Combust. Flame* 111:276 (1997).
16. Shu, Z., Choi, C. W., Aggarwal, S. K., Katta, V. R., and Puri, I. K., *Combust. Flame* 118:91–107 (1999).
17. Katta, V. R., Goss, L. P., and Roquemore, W. M., *Combust Flame* 96:60 (1994).
18. Domingo, P., and Vervisch, L., *Proc. Combust. Inst.* 26:233 (1996).
19. Aggarwal, S. K., and Puri, I. K., *AIAA J.* 36:1190 (1998).
20. Peters, N., in *Reduced Kinetic Mechanisms for Applications in Combustion Systems, Lecture Notes in Physics* (N. Peters and B. Rogg, Eds.), Springer–Verlag, 1993, Vol. 15, pp. 3–14.
21. Puri, I. K., Aggarwal, S. K., Ratti, S., and Azzoni, R., *Combust. Flame* 124:311–325 (2001).
22. Shu, Z., A Numerical Investigation of Steady and Unsteady Methane-Air Partially Premixed Flames, Ph.D. Thesis, University of Illinois at Chicago, 2001.
23. Peters, N., *Proc. Combust. Inst.* 20:353–360 (1984).
24. Seshadri, K., Puri, I. K., and Peters, N., *Combust. Flame* 61:237–249 (1985).
25. Choi, C. W., and Puri, I. K., The Second Joint Meeting of the U. S. Section of the Combustion Institute, San Francisco, 2001
26. Xiao, X., and Puri, I. K., *Appl. Optics* 40:731–740 (2001).

Received 13 June 2001; revised 11 September 2001; accepted 28 September 2001